Influence of Mass loading and inter-particle collisions on particle dispersion in a recirculating flow geometry

J. BORÉE * , T. ISHIMA ** , P. FANOUILLERE*** , I. FLOUR***

* Institut de Mécanique des Fluides ; UMR CNRS/INPT-UPS 5502
Allée du Professeur Camille Soula ; 31400 TOULOUSE ; France

** Gunma University ; Tenjin, KIRYU 376-8515, Japan

*** EDF – DER – LNH , 6, Quai Watier , 76400 CHATOU, France

ABSTRACT

The effect of mass-loading and inter-particle collisions on the development of the polydispersed two-phase flow downstream a confined bluff-body is discussed here. Although the bluff-body flow configuration is one of the simplest turbulent recirculating flows, it is relevant for applications and forms the basis of numerous combusting devices. The present data are obtained for isothermal conditions by using a two-component phase-Doppler anemometer (PDA) allowing size and velocity measurements. A polydispersion of glass beads is introduced in the central tube flow. The statistical properties of narrow particle size classes are displayed and analysed in order to respect the wide range of particle relaxation times. The mean and fluctuating airflow in the presence of glass beads and the statistical properties of the dispersed phase motion have been discussed in a previous paper (Ishima et al. 1998). The data used here form the basis of a validated data set available for model testing.

The influence of mass loading on particle dispersion will be considered in this paper. The initial mass loading M_j of the inner jet is the ratio of the mass flux of particles to the mass flux of air in the jet flow. We propose a correction valid in confined complex 3D flows to ensure that the global mass flux per size class obtained by integration from the PDA data is conserved. The results are used to discuss the strong influence of flow regime on the dispersion of the glass beads. Particles recirculate at the lowest mass loading and the mass concentration of the dispersed phase in the recirculation zone and in the external shear layer is high. This property is interesting for flame stabilisation in two-phase combustion. On the contrary, the memory of the initial jet is detected far downstream at high mass loading and dispersion of particles is reduced dramatically. The signature of inertia effects on the local mean mass distribution of the polydispersion is discussed.

Finally, the effect of inter-particle collisions is considered. Recent applications of kinetic theory to binary mixtures of particles are used to analyse the probability of particle/particle collisions and to emphasise their influence in the stagnation region even at low mass loading. In a polydispersed situation, collisions will result in a redistribution of mean momentum and fluctuating kinetic energy between all colliding particle classes. These effects are observed in the present situation.

1 Introduction

The bluff-body flow configuration is one of the simplest turbulent recirculating flows. It is relevant for applications and forms the basis of numerous combusting devices (Scheffer et al. 1987). We discuss in this paper the effect of mass-loading and inter-particle collisions on the development of the polydispersed two-phase flow downstream a confined bluff-body (figure 1).

The present data are obtained for isothermal conditions by using a two-component phase-Doppler anemometer allowing size and velocity measurements. A polydispersion of glass beads is introduced in the flow. The statistical properties of narrow particle size classes are displayed and analysed in order to respect the wide range of particle relaxation times. The mean and fluctuating airflow in the presence of glass beads and the statistical properties of the dispersed phase motion have been discussed in a previous paper (Ishima, Borée et al. 1998). The data used here form the basis of a validated data set available for model testing (Ishima et al. 1999). As the development of the continuous and dispersed phase velocity fields is concerned, we have shown that the bluff-body flow is very sensitive to initial mass loading M_j of the inner jet - M_j is the ratio of the mass flux of particles to the mass flux of air in the jet flow. An increase in mass loading corresponds to an increase in momentum flux ratio between central jet and annular flow. In the present situation, this implies a complete reorganisation of the recirculation zone and of the turbulent field: In single phase flow (see the sketch of figure 1) and at $M_j = 22\%$, the momentum ratio is smaller than one and the jet stagnates in the recirculation region ; on the contrary, at $M_j = 110\%$, the jet penetrates through the recirculating zone (see figures 2a and 2b). No accurate prediction of this particle-laden flow can therefore be achieved without considering two-way coupling for the partly responsive glass beads.

The influence of mass loading on particle dispersion will be considered in this paper. We therefore need to estimate the evolution of mass fluxes and mass concentration from the PDA data. Such information is very difficult to obtain with PDA (Qiu and Sommerfeld 1992; Sommerfeld and Qiu 1995). In part 3, we propose a correction valid in confined complex 3D flows to ensure that the global mass flux per size class obtained by integration from the data is conserved. The results are used to discuss the strong influence of flow regime on the dispersion of the glass beads.

Finally, the effect of inter-particle collisions is considered. Recent applications of kinetic theory to binary mixtures of particles are used to analyse the probability of particle/particle collisions and to emphasise their influence in the stagnation region even at low mass loading.

2 Experimental Set-up

2.1 Flow Configuration

The experiment presented here has been performed in the flow loop "Hercule"of EdF-LNH. The vertical axisymmetric air flow downstream the bluff body is shown in figure 1. The outer and inner radius of the annular outer region are respectively $(R_2 = 150\,mm\,;\, R_1 = 75\,mm)$. The maximum velocity of the annular flow is 6 m/s and the Reynolds number of the flow is $Re \approx 20000$. The external volume flux is kept constant at $Q_e = 780\ m^3/h$. The length of the straight annular section upstream the test section is $L_e = 2m$. Several honeycomb structures are added in order to remove any swirl motion. An inner tube jet $(R_j = 10mm; U_j(r=0) = 4m/s)$ is generated by compressed air flows on the axis of the recirculation as shown in figure 1. With $2L_e/D_j = 100$, the tube flow is established. The volume flux of the jet is $Q_j = 3.4\,m^3/h$. This corresponds to a mean velocity $\overline{U_j} = 3.4\,m/s$. The ratio of the jet volume flux to the annular flow volume flux is very low (0,5%). The mean velocity was chosen in order to get a single phase flow with stagnation points in the recirculation. The Reynolds number of the pipe flow is $Re \approx 4500$, the flow is turbulent with $\overline{U}_j/U_j(r=0) = 0,85$.

A particular care was devoted to seed both outer and inner single phase flows (Ishima et al. 1998). The test section is 1500 mm in length. For further descriptions, The origin is set on the edge of the bluff body and at the centre of the inner jet. The measurements on the axis were made at 3mm, 10mm, 20mm and after every 20mm up to 500mm. Flow characteristics were also measured in planes of 3, 80, 160, 200, 240, 320 and 400mm. The flow will be described henceforth using a cylindrical coordinate system (x,r,θ) to indicate the axial (downward), radial and azimuthal directions. The components of the mean and fluctuating velocity field are denoted respectively by (U,V,W) and (u,v,w) where V is the radial component and W is the azimuthal component. No swirling motion was detected to within our

measurement precision. Subscripts “f” and “p” indicate respectively fluid and particles properties. The symbol $< >_f$ and $< >_p$ indicates averaging operators associated respectively to fluid and particle phases. The expressions u’ and v’ stand respectively for longitudinal and radial standard deviation.

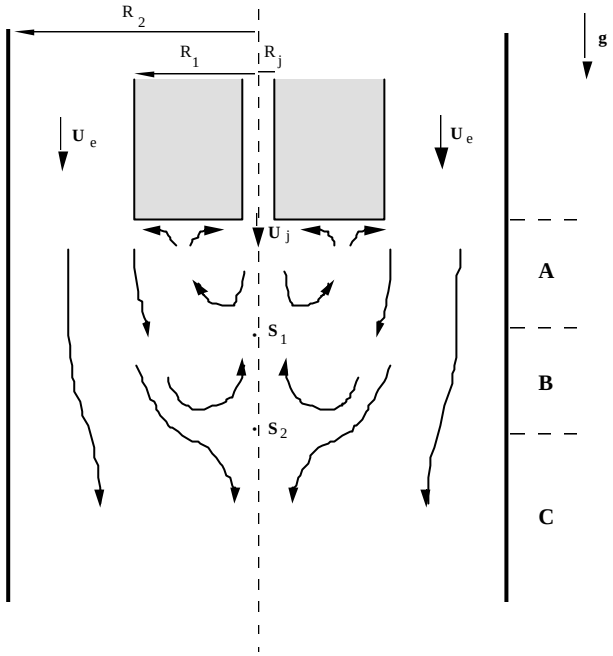

Figure 1 : Sketch of the confined bluff body flow in single phase configuration.

2.2 Glass Particles

Glass particles are released in the conducting pipe of the inner jet by a particle feeder. All flow conditions and particle mass loading are monitored on a work station. The mass loading is controlled accurately in closed loop by weighting continuously the particle feeder. Two mass flux of particles of 1 kg/h (resp. 5 kg/h) corresponding to contrasted inner jet mass loading ratio M_j of $M_j = 22\%$ (resp. $M_j = 110\%$) have been selected in order to show the coupling between continuous and discrete phases. Note that the mass loading ratio of the global flow is in each case very weak: $M_t = 0,1\%$ (resp. $M_t = 0,5\%$).

The material density of the glass particle is $r_p = 2470$ kg/m3. The initial particle size distribution covers a wide range of size classes from 20 µm to 110 µm with a mass averaged diameter of 63 µm. The Stokes number of a particle size class is defined as the ratio of the particle aerodynamic time constant t_p to an appropriate turbulent time scale t_j. The Stokesian particle relaxation time was chosen for $r_p >> r_f$: $t_p = r_p d_p^2 / 18\mu$ where d_p is the median diameter of the particle size class, r_p is the particle density and μ is the fluid viscosity. The particle time scale varies significantly. For size classes 20 µm, 60 µm and 110 µm, its value is respectively $t_p = 3\,ms$; $27\,ms$ and $t_p = 76\,ms$.

2.3 PDA Settings

For making measurements with a Laser Doppler system, 15 optical windows consisting of thin plastics sheets with a thickness of 0.3 mm are located along the test section. A two components phase Doppler anemometer produced by Dantec (particle Dynamics Analyser: PDA) was used. For accuracy and convenience of the displacement, optical fibber system was prefered. Total inter section angle of incident beam was 1.5 degree. The receiving optics was settled at 67 degrees of off-axis angle from the incident beam to minimise the contribution of the reflected light.

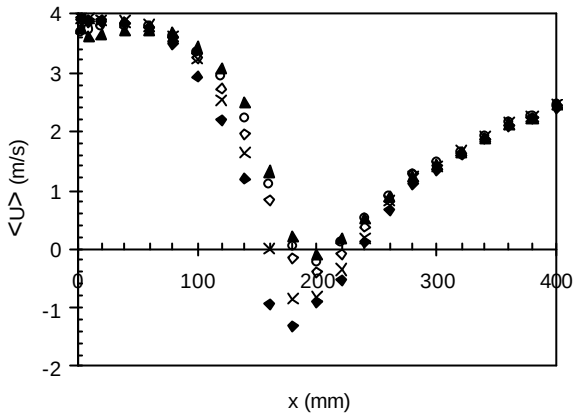

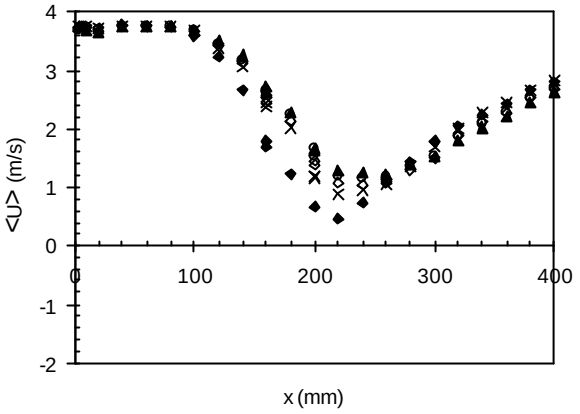

figure 2a (left) and 2b (right) : Axial evolution of the mean longitudinal velocity of continuous and dispersed phase at $M_j = 22\%$ (left) and $M_j = 110\%$ (right)

? , Tracers ; X, $d_p = 20mm$; ? , $d_p = 40mm$; ? , $d_p = 60mm$; ? , $d_p = 80mm$

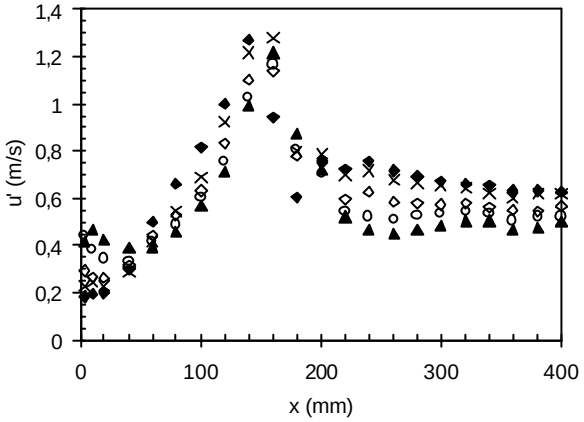

figure 3 : Axial evolution of the axial fluctuating velocity of continuous and dispersed phase at $M_j = 22\%$? , Tracers ; X, $d_p = 20mm$; ? , $d_p = 40mm$; ? , $d_p = 60mm$; ? , $d_p = 80mm$

The optical windows were put only on the incident beam side. The actual off-axis angle was therefore changed from the 67 degree at the outer side of the measuring range because of the refraction effect on the cylindrical wall of the test section. The off-axis angle error by this reason was checked before making diameter measurement. It is less than 3% and is thus not significant for diameters measurements.

Measurements are carried out for the continuous and dispersed phases simultaneously (Ishima, Borée et al. 1998). Unless specified, we perform statistical averaging of at least one thousand independent samples in each size-class. Consequently, estimated statistical absolute errors for mean values (resp. relative errors for standard deviation values) are respectively $\Delta U \approx 0.06u'$ (resp. $E_s \approx 5\%$) with a 95% confidence level.

3 Computation of corrected mass fluxes and mass concentrations

During the measurement time t_m, for the size class i $\left(d_p \in \left[d_{pi}, d_{pi}+dd\right]\right)$ and the velocity class k $\left(\mathbf{U} \in \left[\mathbf{U}_{ik}, \mathbf{U}_{ik}+d\mathbf{u}\right]\right)$, the following simple relations hold for $C_{m\,ik}\left(kg/m^3\right)$, the mean mass concentration of particles per unit volume and $f_{m\,ik}{}^{(n)}\left(kg/m^2 s\right)$ the mean mass flux of particles in direction (n) :

$$t_m.\left\|\mathbf{U}_{ik}\right\|.A_{ik}.C_{m\,ik} = m_i.N_{ik} = m_i.N_{ik}{}^d/h_{ik} \tag{1}$$

$$f_{m\,ik}{}^{(n)} = C_{m\,ik}.\left(\mathbf{U_{ik}}.\mathbf{n}\right) \tag{2}$$

m_i is the mass of particles of class i. ; A_{ik} is the surface of the measurement volume seen by particles of diameter class i and velocity class k ; N_{ik} is the total number of particles of diameter class i and velocity class k flowing through the measurement surface during t_m ; $N_{ik}{}^d$ is the total number of particles of diameter class i and velocity class k detected by PDA during t_m ; h_{ik} is the ratio between $N_{ik}{}^d$ and N_{ik} i.e. $h_{ik} \in [0,1]$. This ratio takes into account the occurrence of non validated samples.

We obtain :

$$C_{m\,ik} = \frac{m_i.N_{ik}{}^d}{h_{ik}.t_m.\left\|\mathbf{U}_{ik}\right\|.A_{ik}} = \frac{1}{h_{ik}A_{ik}}\sum_{j=1}^{N_{ik}{}^d}\frac{m_i}{\left\|\mathbf{U}_{ikj}\right\|.t_m} \tag{3}$$

$$f_{m\,ik}{}^{(n)} = C_{m\,ik}.\left(\mathbf{U_{ik}}.\mathbf{n}\right) = \frac{1}{h_{ik}A_{ik}}\sum_{j=1}^{N_{ik}{}^d}\frac{m_i.\left(\mathbf{U_{ikj}}.\mathbf{n}\right)}{\left\|\mathbf{U}_{ikj}\right\|.t_m} \tag{4}$$

At the exit of the tube in the present study or more generally in quasi parallel turbulent flows of moderate turbulent intensity, one velocity class is considered and these relations are classically simplified with $\left\|\mathbf{U}_{i1\,j}\right\| \approx < U_1 >_{pi}$ (direction (1) is the longitudinal direction) to obtain :

$$f_{m\,i}{}^{(1)} = \frac{1}{h_i A_i}\left(\frac{m_i N_i^d}{t_m}\right) = C_{m\,i}.< U_1 >_{pi} \tag{5}$$

This statement is not true in complex 3D flows of high turbulence intensity. A summation over the velocity space is then necessary with :

$$C_{m\,i} = \sum_k\left(\frac{1}{h_{ik}A_{ik}}\sum_{j=1}^{N_{ik}{}^d}\frac{m_i}{\left\|\mathbf{U}_{ikj}\right\|.t_m}\right) \tag{6}$$

$$f_{m\,i}{}^{(n)} = \sum_k\left(\frac{1}{h_{ik}A_{ik}}\sum_{j=1}^{N_{ik}{}^d}\frac{m_i.\left(\mathbf{U_{ikj}}.\mathbf{n}\right)}{\left\|\mathbf{U}_{ikj}\right\|.t_m}\right) \tag{7}$$

We stress that the instantaneous value of the velocity modulus and not the mean velocity modulus is used in these relations. The quantities are therefore defined even at the mean stagnation point and in fact very similar to alternative definitions based on the residence time of particles in the measurement volume (Hardalupas and Taylor 1989; Qiu and Sommerfeld 1992). The factor $\left(1/h_{ik}A_{ik}\right)$ is one of the major unknowns for flux or concentration measurements using PDA. The rejection ratio h_{ik} is not known and eventually varies with the size class. The surface of the measurement volume seen by particles is very strongly dependent on the diameter of the particle class. It depends also to a smaller extend of the direction of the velocity of the incident particle (see (Qiu and Sommerfeld 1992) for a review). Starting from equation (6) and (7) (Sommerfeld and Qiu 1995) have proposed a method in which the maximum amplitude of the Doppler burst and the integral of the energy of the burst above a given threshold have to be registered by PDA. This

method was proved to be reliable even in complex turbulent recirculating flows but is impossible to apply when commercial systems are used. In the method proposed below, a correction based on the global mass balance of the dispersed phase is adopted. To take into account the strong size dependence of these unknown parameters, the local mass flux is corrected independently for each size class for varying size of the measurement surface seen by the receiving optics and for rejected data. The directional dependence of h_{ik} and A_{ik} is not taken into account. For the given PDA configuration, it should however be a correction of second order when compared to the particle size dependence correction.

Relations (6) and (7) then become, N being the total number of detected particles :

$$C_{m\,i} = \frac{1}{h_i A_i} \sum_{j=1}^{N} \frac{m_i}{\left\| \mathbf{U}_{ij} \right\| . t_m} = \frac{C_{m\,i}^{\,*}}{h_i A_i} \tag{8}$$

$$f_{m\,i}^{\,(n)} = \frac{1}{h_i A_i} \sum_{j=1}^{N} \frac{m_i . \left(\mathbf{U_{ij}.n} \right)}{\left\| \mathbf{U}_{ij} \right\| . t_m} = \frac{f_{mi}^{\,*\,(n)}}{h_i A_i} \tag{9}$$

Quantities $C_{m\,i}^{\,*}$ and $f_{mi}^{\,*\,(n)}$ are first computed from the data. In determining the modulus of the velocity $\left\| \mathbf{U_{ij}} \right\| = \sqrt{U_{ij}^{\,2} + V_{ij}^{\,2} + W_{ij}^{\,2}}$, only two components are known from the two-components PDA measurements. The unknown W_{ij} has zero mean value. Assuming further that $w' \approx v'$, an instantaneous value of W_{ij} is determined by a random number generator having a Gaussian pdf and a rms $w' = v'$.

$\dot{M}_i$ (kg/s) : the total mass per second of particles of class i flowing along the set-up is known for a given experiment. It is related to the local mass flux by :

$$\dot{M}_i = \int_0^{R_2} f_{m\,i}^{\,(1)} . 2\pi r . dr \tag{10}$$

where (1) is the longitudinal direction. We suppose now that both ratio of rejected particles and measurement surface are constant all across the profile. This hypothesis is valid when the global mass loading is low, which is true in most of the Bluff-body flow. It can be very crude in dense particle laden flows as more and more particles intercept the beams as we move across the profile. Measurements discussed in this work show that this assumption provides a good evaluation. Using equation (9) and (10), we obtain :

$$\dot{M}_i = \frac{1}{h_i . A_i} \int_0^{R_2} f_{mi}^{\,*\,(1)} . 2\pi r . dr \tag{11}$$

The value of the product $h_i A_i$ that satisfies the global mass conservation equation is thus computed from the measurements and used in relations (8 and 9) in order to obtain the local concentration and mass fluxes. The relative error on the local values of these quantities can be estimated and is of order $E \approx 10\%$.

4 Effect of mass loading on the dispersion of the glass beads.

To evidence the effect of mass loading on particle dispersion, the radial profiles of mean longitudinal mass flux $f_{mi}^{(1)}$ and mean mass concentration C_{mi} are presented respectively in figure 4 and figure 5. Data relative to the 60 µm size class only are presented for clarity. The right hand side of figure 4 and figure 5 corresponds to $M_j = 22\%$ while the left-hand side corresponds to $M_j = 110\%$. To obtain a direct comparison, the high mass loading values are divided by 5. Both sides therefore artificially correspond to the same initial mean mass flux and mean mass concentration.

For both situations, the signature of the jet, recirculation region and outer shear layer is clear at the axial position $x = 80\ mm$. The high value of $f_{mi60}^{(1)}$ on the axis is not reported in figure 4a in order to focus on the recirculating

region. On the axis and at $x = 80\,mm$, the longitudinal mass flux at $M_j = 22\%$ (resp. $M_j = 110\%$) is $f_{mi60}^{(1)} = 0.29\,kg/m^2\,s$ (resp. $f_{mi60}^{(1)} = 1.1\,kg/m^2\,s$). As relative values are used, figure 4a shows that the relative mean longitudinal mass flux directed upstream in the recirculating region and downstream in the outer shear layer is much more intense at the lowest mass loading. In figure 5a we see very clearly that the mean mass concentration is approximately constant in the recirculating region at $x = 80\,mm$ and reaches a local maximum in the outer shear layer again more pronounced at $M_j = 22\%$. This property is particularly important for flame stabilisation in combusting situation (Hardalupas et al. 1994).

Figure 4a

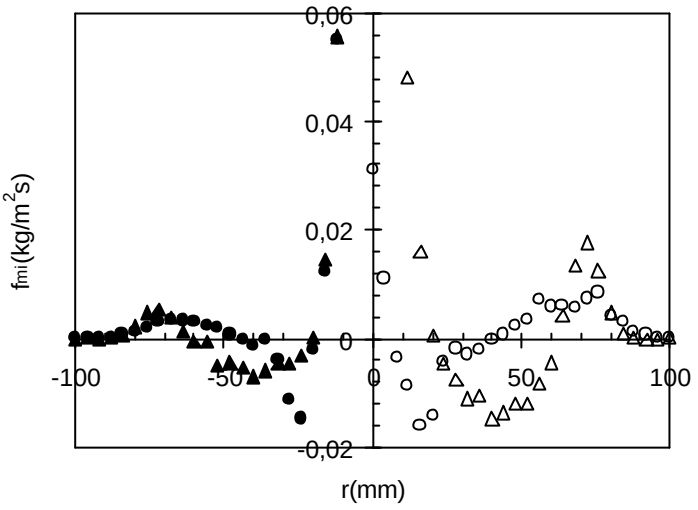

Figure 4b

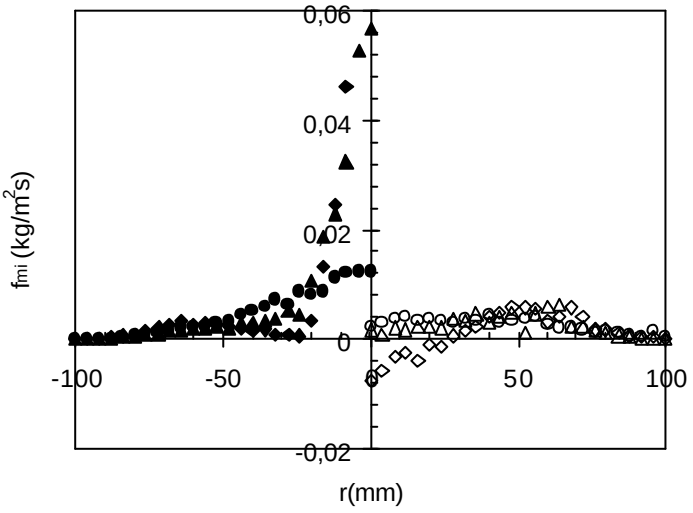

Figure 4 : Radial profiles of mean longitudinal mass flux f_{mi} (Right hand side and open symbols: $M_j = 22\%$; Left hand side and dark symbols: $M_j = 110\%$ and $f_{mi}/5$)

4a : ? and ? , $x = 80\,mm$; ? and ? , $x = 160\,mm$

4b : ? and ? , $x = 200\,mm$; ? and ? , $x = 240\,mm$; ? and ? , $x = 320\,mm$

Figure 5a

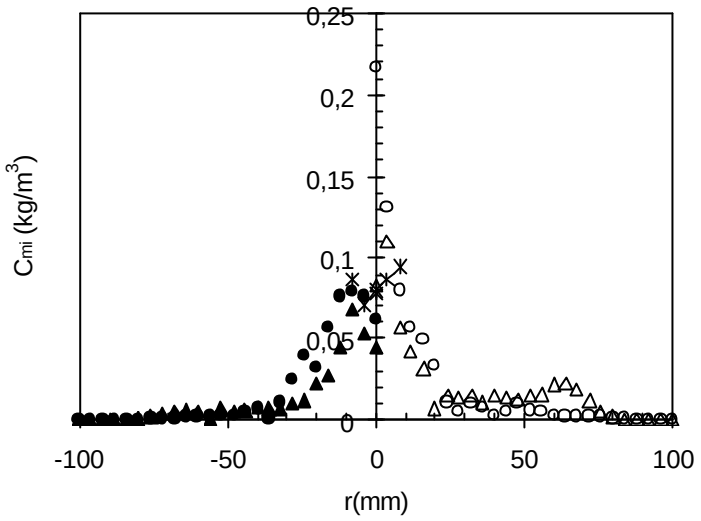

Figure 5b

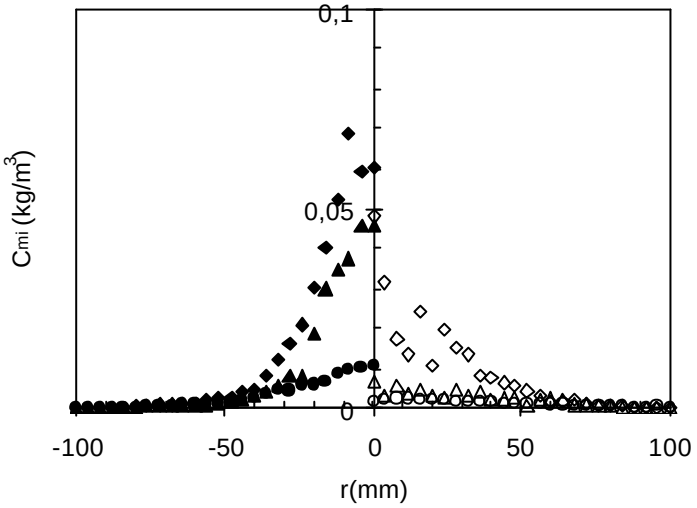

Figure 5 : Radial profiles of mean mass concentration C_{mi} (Right hand side and open symbols: $M_j = 22\%$; Left hand side and dark symbols: $M_j = 110\%$ and $C_{mi}/5$)

5a :* , $x = 3mm$; ? and ? , $x = 80\,mm$; ? and ? , $x = 160\,mm$

5b :? and ? , $x = 200\,mm$; ? and ? , $x = 240\,mm$; ? and ? , $x = 320\,mm$

The station $x = 160\ mm$ is located slightly upstream the mean stagnation point of 60 µm particles (figure 2) at the lowest mass loading. In figure 4a , we see accordingly that $f_{mi60}^{(1)}$ is small on the axis. Moreover, the local mean mass concentration of particles measured at this station is three time greater than the initial mean mass concentration on the axis for $M_j = 22\%$ (figure 5a). Such behaviour is natural near a stagnation point; it is not observed at $M_j = 110\%$. In this case, the jet is still present near the axis at $x = 160\ mm$ and the moderate increase of C_{mi60} is due to the mean velocity decrease.

The contrast between the two situations is evident further downstream. At $M_j = 22\%$, the main result is here that the recirculating region detected at $x = 200\ mm$ is responsible for an efficient radial dispersion of the glass beads. The

profiles of $f_{mi60}{}^{(1)}$ and of C_{mi60} are indeed very flat all across the wake of the bluff-body (right-hand side of figure 4b and figure 5b). At $M_j = 110\%$, a strong decrease of near axis mass flux and concentration also occur at the end of the off-axis-recirculated region. The signature of the jet is however detected far downstream. These results show the interest of configurations with stagnation point on axis.

Such a discussion could be performed for other size classes. Similar conclusions would be reached qualitatively. Contrasted size classes however imply quantitatively a different behaviour that have an important signature on the local mean mass distribution of the polydispersion (not shown here). A striking effect of axial recirculating region is detected at the lowest mass loading. $x = 200\ mm$ corresponds to a very low mean velocity of the large size classes in the recirculation zone and therefore to a very high mean mass concentration for these classes. Accordingly, the mass averaged diameter of the polydispersion at $x = 200\ mm$ is $\overline{d_{p_M}} = 78\ mm$. This value is 24% higher than the initial value $\overline{d_{p_M}} = 63\ mm$. At the exit of the measurement domain ($x = 400\ mm$) and at $M_j = 22\%$, the mass averaged diameter of the polydispersion is $\overline{d_{p_M}} = 69\ mm$. This value is larger than the initial value because small size classes disperse more efficiently.

On high mass loading results, we see a continuous shift of the mean mass frequency distribution on the axis toward large size classes that disperse less efficiently. Inertia effects more pronounced for large size classes in the turbulence of the penetrating jet are also responsible for this observation. Noticeably, mass frequency distributions drawn at the same axial locations but at $r = 76\ mm$, i.e. aligned with the edge of the bluff body in the outer shear layer, show an opposite trend with a continuous shift of the mean mass distribution toward small size classes that disperse more efficiently.

5 On the effect of particle/particle collisions.

In a polydispersed particle laden flow, the probability of collision between a particle of size class "i" and the class "j" depends on particle "j" concentration, particles sizes, mean slip motion and fluctuating motion of both classes. The importance of collisions on the motion of a given size class "i" is evaluated by computing the ratio N_{Ci} of the averaged time between collisions t_{Ci} to the particle response time t_{pi}. $N_{Ci} \leq 1$ corresponds to a situation in which collisions cannot be neglected. Only binary collisions are considered here. The frequency of collisions $f_{Ci} = 1/t_{Ci}$ is therefore computed as the sum of the frequency of collisions with each size class $f_{Ci} = \sum_{class} f_{Ci,j}$. The correlation of the velocities of colliding particles is not taken into account for the present evaluation and results valid in the kinetic theory limit are used (Abrahamson 1975). To take into account both collisions due to fluctuating motion and collisions due to mean drift between particles, $f_{Ci,j}$ is taken as the sum of two asymptotic situations corresponding respectively to turbulent fluctuations and low mean drift $f_{TCi,j}$ and to high drift $f_{DCi,j}$ (Gourdel et al. 1998) with :

$$f_{Ci,j} = f_{TCi,j} + f_{DCi,j} \tag{12}$$

$$f_{TCi,j} = 2^{2/3} p^{1/2} n_j \left(R_{pi} + R_{pj}\right)^2 \sqrt{s_{pi}{}^2 + s_{pj}{}^2} \tag{13}$$

$$f_{DCi,j} = p\, n_j \left(R_{pi} + R_{pj}\right)^2 \left\| U_{pi} - U_{pj} \right\| \tag{14}$$

In relations (13) and (14), R_p is the radius of the particle, n_j is the number concentration for class j deduced from mass concentration measurements and $s_{pi}{}^2$ is the averaged fluctuating component: $s_{pi}{}^2 = \left(u_{pi}{}^2 + v_{pi}{}^2 + w_{pi}{}^2\right)/3 = \left(u_{pi}{}^2 + 2.v_{pi}{}^2\right)/3$ on the axis of the axisymmetric flow.

The averaged time between collisions t_{Ci} at different axial locations is compared in figure 6a and 6b with the Stokesian time scale of the particles. We note that t_{Ci} decreases sharply as the diameter of the particle increases. An analysis based on a mean diameter would be inaccurate. At low mass loading (figure 6a) and at the exit of the jet $(x = 3mm)$, the role of particle/particle collisions is expected to be of minor importance as only the largest size classes, which have a large inertia and a low number density, are expected to collide with other particles. The probability of collisions however increases when ones moves downstream and is very high for most classes about the mean stagnation point $(x \approx 160\,mm)$. This is obviously very different from free jet behaviour. Finally, figure 6a shows that collisions are not probable downstream the recirculation zone where particles are well dispersed. At the highest mass loading studied here (figure 6b) large size classes are expected to be influenced by inter-particle collisions at the jet exit and in the inner jet along all off-axis recirculated region. For all size classes, t_{Ci} is again much smaller in regions of high fluctuating intensity.

In the recirculating flow geometry, (i) the very high level of turbulent fluctuations (see figure 3) ; (ii) the non-negligible inter-class particle mean slip velocity (see figure2a and 2b) and (iii) the increase of mean mass concentration if the jet stagnates enhance the probability of collisions. At the lowest mass loading, the spatial extend of the region where collisions are probable is however small and confined near the stagnation point. Collisional terms should have only a weak influence on the development of the flow. The situation is not the same at the highest mass loading as collisions between large size classes are probable all along the jet flow to the downstream end of the recirculation zone. Noticeably, the mean drift between large size classes is more than three time smaller at $M_j = 110\%$ than at $M_j = 22\%$. Even if both mass loading correspond to contrasted aerodynamical situations, this observation is expected to be the result of mean momentum redistribution between all colliding particle classes. Figure 7 compares the evolution of the ratio of the turbulent kinetic energy k_p/k_f where $k = 1/2\left(u'^2 + 2.v'^2\right)$ as a function of the size class on the axis at $x = 240\,mm$. This location has been chosen because it corresponds approximately to the end of the recirculation zone. In both situations, the influence of the jet flow is thus weaker and the radial air turbulent intensity is high (Borée et al. 2000). Particles are therefore under the influence of an intense lateral flapping. One sees clearly however that k_p decreases continuously at $M_j = 22\%$ where no collisions occur while a plateau is observed for $d_p > 40\,mm$ at $M_j = 110\%$. Such evolution should be a direct consequence of redistribution of fluctuating kinetic energy between all colliding particle classes.

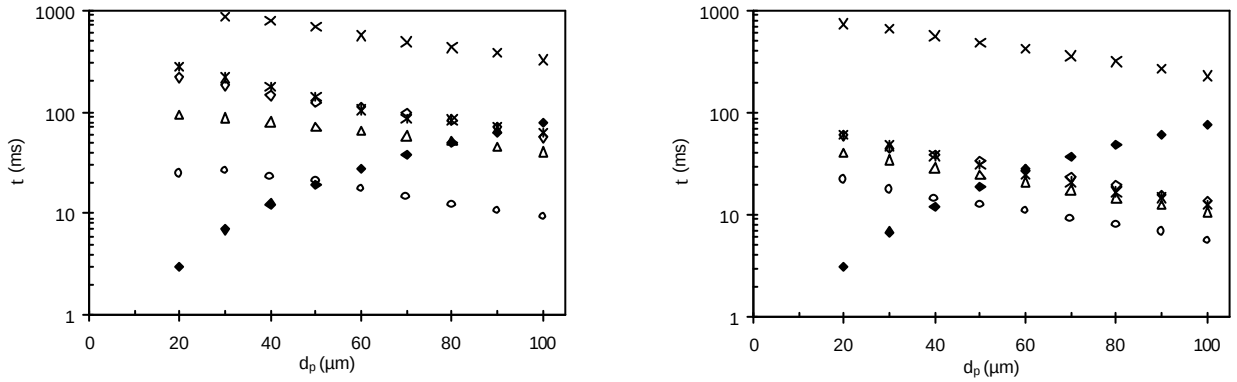

figure 6a (left) and 6b (right) : Comparison between the average time between collisions and the particle response time at different stations along the axis.

6a : $M_j = 22\%$. ? , t_{pi} ; * , $t_{Ci} : x = 3mm$; ? , $t_{Ci} : x = 80\,mm$; ? , $t_{Ci} : x = 160\,mm$; ? , $t_{Ci} : x = 200\,mm$; X, $t_{Ci} : x = 240\,mm$

6b : $M_j = 110\%$? , t_{pi} ; * , $t_{Ci} : x = 3mm$; ? , $t_{Ci} : x = 80\,mm$; ? , $t_{Ci} : x = 160\,mm$; ? , $t_{Ci} : x = 240\,mm$; X, $t_{Ci} : x = 320\,mm$

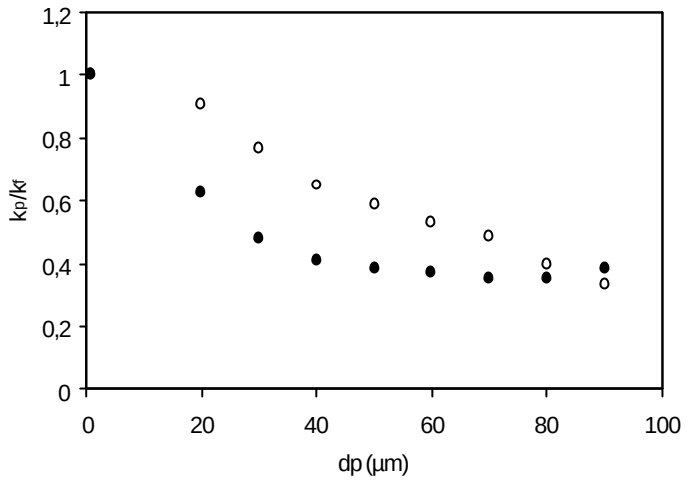

figure 7 : Evolution of the ratio of the turbulent kinetic energy k_p/k_f as a function of the size class on the axis at $x = 240\,mm$. ?, $M_j = 22\%$; ? , $M_j = 110\%$.

6. Conclusion

The influence of mass-loading and inter-particle collisions on the dispersion of solid particles in a recirculating flow geometry was discussed in this paper. The bluff-body flow configuration considered here is one of the simplest turbulent recirculating flows. It is also relevant for applications and forms the basis of numerous combusting devices.

The present data were obtained for isothermal conditions by using a phase-Doppler anemometer allowing size and velocity measurements. A polydispersion of glass beads is introduced in the flow. The statistical properties of narrow particle size classes are displayed and analysed in order to respect the wide range of particle relaxation times.

In order to educe the spatial evolution of mass-fluxes and mass concentration per size class, a correction was introduced to the PDA data to ensure that the global mass flux per size class obtained by integration from the data is correct. This information provides a rich understanding of the two-phase flow. We show that the sensitivity to mass loading deeply affects the dispersion of the glass beads. Particles recirculate at the lowest mass loading and the mass concentration of the dispersed phase in the recirculation zone and in the external shear layer is high. This property is interesting for flame stabilisation in two-phase combustion. The recirculation at $M_j = 22\%$ is also shown to be efficient to disperse radialy the particles in the downstream wake of the bluff-body. On the contrary, the memory of the initial jet is detected far downstream at $M_j = 110\%$ and dispersion of particles is reduced dramatically. Moreover, contrasted size classes imply quantitatively a different behaviour that have an important signature on the local mean mass distribution of the polydispersion. As an example, the measured the mass averaged diameter of the polydispersion is 25% higher than its initial value in the stagnation region at $M_j = 22\%$.

Recent application of the kinetic theory to binary mixture of particles was applied to the polydispersed situation to evaluate the probability of collision for a given size class. The longitudinal increase of both particle number density and turbulent fluctuations downstream the inner jet imply a very high probability of collisions for the major size classes of the polydispersion in the mean stagnation region even at $M_j = 22\%$. In contrast, collisions are seen to be very probable all along the jet flow at the highest mass loading. In a polydispersed situation, collisions will result in a redistribution of mean momentum and fluctuating kinetic energy between all colliding particle classes. These effects are observed in the present situation.

Acknowledgements

We want to express a special acknowledgement to O. Simonin for many fruitful discussions and for launching this research. We thank G. Balzer and B. Martelet, successive heads of the research group G.E.I.D.R. of EdF - R&D who accepted to keep on the long way necessary to obtain reliable experimental results.

References

Abrahamson (1975). "Collision rates of small particles in a vigorously turbulent fluid." Chem. Eng. Sci. **30**: 1371-1379.

Borée, J., T. Ishima and I. Flour (2000). "The effect of mass loading and inter-particle collisions on the development of the polydispersed two-phase flow downstream a confined bluff body." Paper submitted to Journal of Fluid Mechanics.

Gourdel, C., O. Simonin and E. Brunier (1998). Modelling and simulation of gas-solid turbulent flows with a binary mixture of particles. Third International Conference on Multiphase Flows, ICMF'98, Lyon, June 8-12.

Hardalupas, Y., C. H. Liu and J. H. Whitelaw (1994). "Experiments with disk stabilised kerosene-fuelled flames." Combust. Sci. and Tech. **97**: 157-191.

Hardalupas, Y. and A. K. M. P. Taylor (1989). "On the measurement of particle concentration near a stagnation point." Exp. in Fluids **8**: 113-118.

Ishima, T., J. Borée, P. Fanouillère and I. Flour (1998). Experimental analysis of a confined bluff body flow laden with polydispersed solid particles. Selected paper of Ninth International Symposium on applications of Laser techniques to Fluid Mechanics, Lisbon.

Ishima, T., J. Borée, P. Fanouillère and I. Flour (1999). Presentation of a data base obtained in a confined bluff body flow laden with polydispersed solid particles. 9th workshop on Two Phase Flow Predictions (http://www-mvt.iw.uni-halle.de/mvt-home.html), Merseburg, April 13-16.

Qiu, H. H. and M. Sommerfeld (1992). "A reliable method for determining the measurement volume size and particle mass fluxes using phase-Doppler anemometry." Experiments in fluids **13**: 393-404.

Scheffer, R. W., J. Kelly and M. Namazian (1987). "Velocity Measurements in a Turbulent Nonpremixed Bluff-Body Stabilized flames." Comb. Sci. and Tech. **56**: 101-138.

Sommerfeld, M. and H. H. Qiu (1995). "Particle concentration measurements by phase-doppler anemometry in complex dispersed two-phase flows." Experiments in fluids **18**: 187-198.